Bardeen spacetime as a quantum corrected Schwarzschild black hole: Quasinormal modes and Hawking radiation

R. A. Konoplya[*] and D. Ovchinnikov[†]

Research Centre for Theoretical Physics and Astrophysics, Institute of Physics, Silesian University in Opava, Bezručovo náměstí 13, CZ-74601 Opava, Czech Republic

B. Ahmedov[‡]

Ulugh Beg Astronomical Institute, Astronomy Street 33, Tashkent 100052, Uzbekistan; Institute of Fundamental and Applied Research, National Research University TIIAME, Kori Niyoziy 39, Tashkent 100000, Uzbekistan; and Institute of Theoretical Physics, National University of Uzbekistan, Tashkent 100174, Uzbekistan

(Received 29 July 2023; accepted 22 October 2023; published 27 November 2023)

The Bardeen black hole holds historical significance as the first model of a regular black hole. Recently, there have been proposed interpretations of the Bardeen spacetime as quantum corrections to the Schwarzschild solution. Our study focuses on investigating the quasinormal modes and Hawking radiation of the Bardeen black hole. We have observed that previous studies on the quasinormal modes for the Bardeen black hole suffer from inaccuracies that cannot be neglected. Therefore, we propose accurate calculations of the quasinormal modes for scalar, electromagnetic, and neutrino fields in the Bardeen spacetime. Additionally, we have computed the gray-body factors and analyzed the emission rates of Hawking radiation. Even when the quantum correction is small and the fundamental mode only slightly differs from its Schwarzschild value, the first several overtones deviate at an increasingly stronger rate. This deviation leads to the appearance of overtones with very small real oscillation frequencies. This outburst of overtones is closely linked to the fact that the quantum-corrected black hole differs from its classical limit primarily near the event horizon. Moreover, the intensity of the Hawking radiation is significantly suppressed (up to 3 orders of magnitude) by the quantum correction.

DOI: 10.1103/PhysRevD.108.104054

I. INTRODUCTION

The problem of a central singularity in the Schwarzschild solution represents a limitation of Einstein's theory of gravity. Consequently, the development of regular black hole models within various approaches and theories of gravity has become an important endeavor. The Bardeen black hole stands as the first historically significant *ad hoc* model describing a regular black hole [1]. Subsequently, an interpretation of the Bardeen metric was proposed in the context of a specific nonlinear electrodynamics in curved spacetime, positing it as a giant gravitating magnetic monopole [2]. However, if the weak field limit is reduced to the usual Maxwell electrodynamics, the electric charge must vanish, as per the Bronnikov theorem [3]. Despite such an exotic interpretation of the Bardeen spacetime, numerous studies have been dedicated to exploring various effects around magnetic monopoles, particularly their characteristic oscillation frequencies known as *quasinormal modes* [4–24].

Quasinormal modes not only serve as fundamental observables that characterize black holes [25], but also play a crucial role in gauge/gravity duality for describing strongly coupled quantum systems [26], as well as in determining the (in)stability of black holes [27].

However, a significant portion of the aforementioned quasinormal mode calculations for the Bardeen black hole suffer from considerable numerical inaccuracies due to the utilization of various approximations. Consequently, it becomes necessary to reexamine some of these results using accurate methods based on converging procedures, such as the Leaver methods [28].

Nevertheless, the focus of our investigation here is on the Bardeen spacetime not within the context of an exotic nonlinear electrodynamics, but rather as a quantum-corrected solution to the Schwarzschild spacetime. In this framework, the parameter that formerly represented the magnetic charge now controls the magnitude of the quantum correction for a neutral black hole. Remarkably, stringy corrections to Schwarzschild black hole spacetimes arising

[*]roman.konoplya@gmail.com
[†]dmitriy.ovchinnikov@physics.slu.cz
[‡]ahmedov@astrin.uz

from string T duality were proposed in [29]. As an initial step, the static Newtonian potential was derived by exploiting the relationship between T duality and path integral duality. Subsequently, it was demonstrated that the intrinsic nonperturbative nature of stringy corrections introduces an ultraviolet cutoff known as the zero-point length, resulting in a regular static potential. This finding was employed to derive a consistent black hole metric for a spherically symmetric, electrically neutral regular black hole, which is equivalent to the Bardeen spacetime after redefinition of constants. It is noteworthy that a similar duality is utilized to probe the quantum fluctuations of the background spacetime [30]. Ultimately, the Bardeen spacetime can also be deduced as an effective metric that reproduces the thermodynamics of a black hole within the generalized uncertainty principle [31], which represents another, more speculative approach to uncovering quantum corrections.

In this paper, we will investigate the quasinormal modes of scalar, electromagnetic, and neutrino fields in the background of the Bardeen spacetime, considering its aforementioned interpretation as a neutral quantum-corrected black hole. Our aim is to demonstrate the inaccuracies present in some of the previous calculations within certain parameter ranges. Here, we present precise calculations not only for the fundamental mode but also for the initial overtones with $\ell \leq n$, where ℓ represents the multipole number and n denotes the overtone number. While it is commonly believed that the fundamental mode suffices as a fingerprint of the black hole, this is not entirely accurate. The fundamental mode is insensitive to the geometry of the event horizon and is primarily determined by the geometry near the peak of the effective potential. Consequently, if a black hole were to be replaced by a wormhole with the same geometry near the potential's peak, the fundamental mode would exhibit minimal change [32,33]. To ascertain the near-horizon behavior, it is necessary to consider multiple overtones [34], which also characterize the early phase of the ringdown [35]. Therefore, studying the initial few overtones will enable us to probe the geometry of the black hole in the vicinity of the event horizon.

We will demonstrate that the overtones deviate from their Schwarzschild limits at a significantly higher rate than the fundamental mode, and this deviation stems from the deformation of the metric near the event horizon [34]. Similar outbursts have recently been observed in the context of black holes in higher-curvature corrected theories and asymptotically safe gravity [36–39].

Quantum-corrected black holes are expected to undergo intense Hawking evaporation, making it crucial to investigate Hawking radiation in the vicinity of Bardeen black holes. To the best of our knowledge, a comprehensive study of Hawking evaporation in this context has not yet been proposed.

In this paper, we will explore Hawking radiation of massless Standard Model fields around Bardeen black holes and demonstrate that the quantum correction significantly reduces the energy emission rate of the test fields (up to 3 orders of magnitude). To determine the emission rates, we will solve the problem of field scattering around the black hole, specifically by calculating the gray-body factors that account for the reflection from the effective potential and diminish the total emission rate.

The paper is organized as follows. In Sec. II, we provide a brief review of the Bardeen solution and the corresponding wavelike equations with effective potentials. In Sec. III, we describe the numerical methods employed to calculate quasinormal modes and gray-body factors, including the WKB approach, accurate Frobenius method, and time-domain integration. Section IV is dedicated to discussing the obtained quasinormal modes and the outburst of overtones. In Sec. V, we present the results of the calculations for gray-body factors and energy emission rates in Hawking radiation. Finally, in the Conclusions section, we summarize the obtained results and mention some open problems.

II. BARDEEN SPACETIME AND THE WAVELIKE EQUATIONS

The Bardeen spacetime is described by the following line element:

$$ds^2 = -f(r)dt^2 + f^{-1}(r)dr^2 + r^2(d\theta^2 + \sin^2\theta d\varphi^2), \quad (1)$$

where

$$f(r) = 1 - \frac{2Mr^2}{(r^2 + l_0^2)^{3/2}}. \quad (2)$$

For $l_0 \neq 0$, the spacetime in Eq. (2) has horizons only if

$$|l_0| \leq \frac{4M}{3\sqrt{3}},$$

as was shown in [40]. The parameter l_0 is related to the Regge slope as follows:

$$\sqrt{\alpha'} = \frac{l_0}{2\pi} \approx 0.117 l_P, \quad (3)$$

where l_P is the Plank mass, so that, as in [30], we have $l_0 \sim l_P$. Stringy effects produce a de Sitter core at the origin, because

$$f(r) \to 1 - \frac{\Lambda_{\rm eff} r^2}{3}, \qquad r \ll l_0, \quad (4)$$

with an effective cosmological constant $\Lambda_{\rm eff} = 6M/l_0^3$. This repulsive effect at small distances stabilizes the matter configuration against collapse.

The general relativistic equations for the scalar (Φ), electromagnetic (A_μ), and Dirac (Υ) fields can be written as follows:

$$\frac{1}{\sqrt{-g}}\partial_\mu(\sqrt{-g}g^{\mu\nu}\partial_\nu\Phi)=0, \tag{5a}$$

$$\frac{1}{\sqrt{-g}}\partial_\mu(F_{\rho\sigma}g^{\rho\nu}g^{\sigma\mu}\sqrt{-g})=0, \tag{5b}$$

$$\gamma^\alpha\left(\frac{\partial}{\partial x^\alpha}-\Gamma_\alpha\right)\Upsilon=0, \tag{5c}$$

where $F_{\mu\nu}=\partial_\mu A_\nu-\partial_\nu A_\mu$ is the electromagnetic tensor, γ^α are gamma matrices, and Γ_α are spin connections in the tetrad formalism. After separation of the variables the above equations (5) take the Schrödinger wavelike form:

$$\frac{d^2\Psi}{dr_*^2}+(\omega^2-V(r))\Psi=0, \tag{6}$$

where the "tortoise coordinate" r_* is defined as follows:

$$dr_*\equiv\frac{dr}{f(r)}. \tag{7}$$

The effective potentials for the scalar ($s=0$) and electromagnetic ($s=1$) fields have the form

$$V(r)=f(r)\frac{\ell(\ell+1)}{r^2}+(1-s)\cdot\frac{f(r)}{r}\frac{df(r)}{dr}, \tag{8}$$

where $\ell=s,s+1,s+2,\ldots$ are the multipole numbers. On the Fig. 1 the effective potential for the Maxwell field is shown. For the Dirac field ($s=1/2$) one has two isospectral potentials,

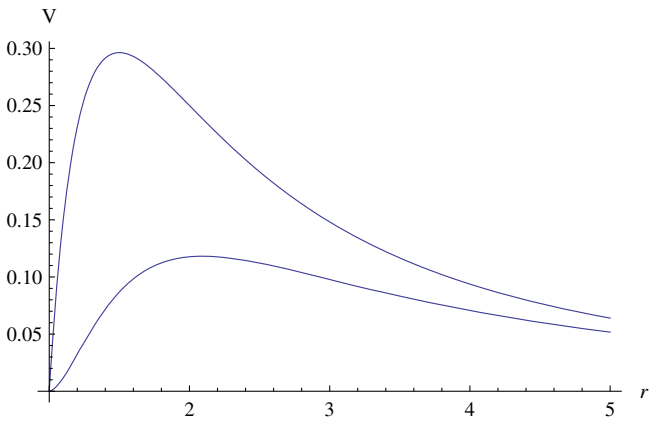

FIG. 1. The effective potential for the $\ell=1$ perturbation of the Maxwell field for the Schwarzschild (bottom) and near extreme Bardeen $l_0=0.7$ (top) black holes; $r_0=1$.

$$V_\pm(r)=W^2\pm\frac{dW}{dr_*},\qquad W\equiv\left(\ell+\frac{1}{2}\right)\frac{\sqrt{f(r)}}{r}. \tag{9}$$

The isospectral wave functions can be transformed one into another by the Darboux transformation

$$\Psi_+=q\left(W+\frac{d}{dr_*}\right)\Psi_-,\quad q=\text{const}, \tag{10}$$

so that it is sufficient to calculate quasinormal modes and gray-body factors for only one of the effective potentials.

III. METHODS FOR FINDING OF QUASINORMAL MODES AND GRAY-BODY FACTORS

Quasinormal modes represent eigenvalues of the wavelike equations mentioned earlier, corresponding to purely outgoing waves at spatial infinity and purely ingoing waves at the event horizon. Since methods for determining quasinormal frequencies have been extensively discussed in numerous papers, we will provide a brief summary of the three methods employed in this study: the WKB approach with Padé approximants, the Leaver method, and time-domain integration. Furthermore, we will discuss the ordinary WKB method's application in finding gray-body factors.

A. WKB approach

We will utilize the semianalytic WKB approach developed by Will and Schutz [41] to determine the quasinormal modes. The Will-Schutz formula has been extended to higher orders [42–44] and improved further by implementing Padé approximants [44,45].

The general form of the WKB formula, as derived by Konoplya [46], is as follows:

$$\omega^2=V_0+A_2(\mathcal{K}^2)+A_4(\mathcal{K}^2)+A_6(\mathcal{K}^2)+\ldots -i\mathcal{K}\sqrt{-2V_2}(1+A_3(\mathcal{K}^2)+A_5(\mathcal{K}^2)+A_7(\mathcal{K}^2)+\ldots), \tag{11}$$

where $\mathcal{K}=n+1/2$ is a half integer. The corrections $A_k(\mathcal{K}^2)$, of order k, in the eikonal formula are polynomials of $\mathcal{K}^2$ with rational coefficients. These corrections depend on the values of higher derivatives of the potential $V(r)$ at its maximum. To enhance the accuracy of the WKB formula, we will follow the approach of Matyjasek and Opala [44] by utilizing Padé approximants. Specifically, we will employ the sixth-order WKB method with $\tilde{m}=4$, 5, where $\tilde{m}$ is defined in [44,46], as this choice yields the best accuracy in the Schwarzschild limit and is also appropriate for the Bardeen black hole, as confirmed by comparisons with accurate data.

It is important to note that the WKB series converges only asymptotically and does not guarantee improved accuracy at each order. Therefore, it is necessary to cross

validate the WKB results with the convergent Frobenius method. Additionally, the outburst of overtones, occurring when $\ell < n$, cannot be captured by the WKB formula in principle. Hence, in this study, we primarily employ the WKB method as an additional check and solely for calculating the fundamental modes.

B. Frobenius method

To obtain precise values of quasinormal modes, including overtones with $\ell < n$, we will utilize the Frobenius method, as initially employed by Leaver for calculating quasinormal modes [28]. The wavelike equation always exhibits a regular singularity at the horizon $r = r_0$ and an irregular singularity at spatial infinity $r = \infty$. To address this, we introduce a new function:

$$\Psi(r) = P(r,\omega)\left(1-\frac{r_0}{r}\right)^{-i\omega/F'(r_0)} y(r). \tag{12}$$

Here, the factor P is chosen such that $y(r)$ is regular for $r_0 \le r < \infty$, ensuring that $\Psi(r)$ corresponds to a purely outgoing wave at spatial infinity and a purely ingoing wave at the event horizon. Consequently, we can express $y(r)$ in terms of a Frobenius series:

$$y(r) = \sum_{k=0}^{\infty} a_k \left(1-\frac{r_0}{r}\right)^k. \tag{13}$$

By employing Gaussian elimination in the recurrence relation for the expansion coefficients, we reduce the problem to solving an algebraic equation. To enhance convergence speed, we will implement the Nollert improvement [47] in its general form for the n-term recurrence relation [48]. When the singular points of the wavelike equation appear within the unit circle $|x| < 1$, we employ a sequence of positive real midpoints as described in [49].

C. Time domain integration

To determine the quasinormal modes and asymptotic tails, we will employ the time-domain integration method. We integrate the wavelike equation using the null-cone variables $u = t - r_*$ and $v = t + r_*$. For the discretization scheme, we will apply the Gundlach-Price-Pullin method [50], which can be expressed as

$$\Psi(N) = \Psi(W) + \Psi(E) - \Psi(S) - \Delta^2 V(S)\frac{\Psi(W)+\Psi(E)}{4} + \mathcal{O}(\Delta^4). \tag{14}$$

Here, the points are denoted as follows: $N \equiv (u+\Delta, v+\Delta)$, $W \equiv (u+\Delta, v)$, $E \equiv (u, v+\Delta)$, and $S \equiv (u, v)$. Gaussian initial data are imposed on the two null surfaces $u = u_0$ and $v = v_0$.

In the course of computations we need to find the effective potential as a function of the tortoise coordinate r_* with great accuracy in order to avoid accumulation of the numerical error. For this purpose one could integrate Eq. (7), find r^* as a function of r, and then use the inverted function to find the effective potential. However, we find that the more economic way is to integrate Eq. (7) as a nonlinear differential equation $r'(r_*) = f(r)$, for example, with the help of the built-in function NDSolve of MATHEMATICA [51], and find $r(r_*)$ with which we can easily construct the effective potential as a function of the tortoise coordinate. More details on the time-domain integration method can be found in a review [27].

The dominant quasinormal frequencies can be extracted from the time-domain profiles using the Prony method [27]. While extracting the frequency from the time-domain profile with high precision can be challenging, the accuracy for the fundamental mode is guaranteed to be sufficiently good.

D. Scattering problem

To investigate Hawking radiation, we will address a different boundary problem that pertains to the scattering of fields in the vicinity of the black hole. Gray-body factors play a crucial role in determining the proportion of initial radiation that gets reflected back to the event horizon by the potential barrier nearby. Subsequently, by employing the Hawking semiclassical formula along with the gray-body factor, we can calculate the amount of radiation that reaches an observer in the far zone. It is worth noting that while temperature is typically the dominant factor in estimating the intensity of Hawking radiation, there are cases where gray-body factors can be equally important [52].

We will examine the wave equations under boundary conditions that permit incoming waves from infinity. Owing to the scattering symmetry, this is equivalent to considering the scattering of a wave originating from the horizon. The boundary conditions for this scattering problem are as follows:

$$\begin{aligned} &\Psi = e^{-i\omega r_*} + Re^{i\omega r_*}, && r_* \to +\infty, \\ &\Psi = Te^{-i\omega r_*}, && r_* \to -\infty. \end{aligned} \tag{15}$$

Here, R and T represent the reflection and transmission coefficients, respectively.

The effective potentials for test Maxwell and Dirac fields have the form of potential barriers which decrease monotonically toward both infinities [53], allowing for application of the WKB approach [41–43] to determine R and T. As ω^2 is real for the scattering problem, the WKB values for R and T will be real as well [41–43], and

$$|T|^2 + |R|^2 = 1. \tag{16}$$

Once the reflection coefficient is obtained, we can find the transmission coefficient for each multipole number ℓ,

$$|\mathcal{A}_\ell|^2 = 1 - |R_\ell|^2 = |T_\ell|^2, \tag{17}$$

where $\mathcal{A}_\ell$ is called *the gray-body factor.*

Here we will use the higher order WKB formula [43] for a relatively accurate calculation of the gray-body factors. However, this formula is not suitable for very small values of ω, which correspond to almost complete wave reflection and have negligible contributions to the overall energy emission rate. For this mode, we employed extrapolation of the WKB results at a given order to smaller ω [54]. According to [41,42], the reflection coefficient can be expressed as follows:

$$R = (1 + e^{-2i\pi K})^{-1/2}, \tag{18}$$

where K is determined by solving the equation

$$K - i\frac{(\omega^2 - V_{\max})}{\sqrt{-2V''_{\max}}} - \sum_{i=2}^{i=6} \Lambda_i(K) = 0, \tag{19}$$

involving the maximum effective potential $V_{\max}$, its second-order derivative $V''_{\max}$ with respect to the tortoise coordinate, and higher order WKB corrections Λ_i. As mentioned above, the WKB series does not guarantee convergence in each order, but only asymptotically, so that usually there is an optimal moderate order at which the accuracy is the best. This order depends on the form of the effective potential. Here we used sixth order for Maxwell perturbations and third order for the Dirac field with a plus potential, because these orders provide the best accuracy in the Schwarzschild limit, and we expect that this will also take place for the Bardeen black hole. This approach was used in a few papers [46,55–57], showing usually reasonably good concordance with the numerical integration. Unfortunately, the Pade approximant, which greatly improves the accuracy when finding quasinormal modes, cannot be used when finding the gray-body factors, because of the nonuniquness of such a procedure.

IV. QUASINORMAL MODES AND THE OUTBURST OF OVERTONES

As a general rule, analytical solutions for quasinormal frequencies of four- and higher-dimensional black holes are not available. However, they can often be obtained in the regime of large multipole numbers ℓ. By utilizing the first-order WKB formula and expanding the position of the maximum of the effective potential, we can derive the following WKB expression for ω in terms of $1/L$ and l_0, where $L = \ell + \frac{1}{2}$:

$$r_{\max} = 3M - \frac{5l_0^2}{6M} - \frac{65l_0^4}{216M^3} + \mathcal{O}(l_0^6) \tag{20}$$

$$\omega = \frac{L}{3\sqrt{3}M} - \frac{i(2n+1)}{6\sqrt{3}M} + l_0^2\left(\frac{L}{18\sqrt{3}M^3} + \frac{i(2n+1)}{54\sqrt{3}M^3}\right) + l_0^4\left(\frac{17L}{648\sqrt{3}M^5} + \frac{7i(2n+1)}{324\sqrt{3}M^5}\right) + \mathcal{O}\left(\frac{1}{L}, l_0^6\right). \tag{21}$$

It is evident that the above expressions are accurate in the limit of large ℓ, while still providing reasonable accuracy even at moderate values of ℓ. When $l_0 = 0$, these analytical formulas reduce to the well-known expressions for the Schwarzschild black hole [58] (see Refs. [59,60] and references therein for various generalizations of these relations). Furthermore, the aforementioned eikonal formula can be derived through the correspondence between eikonal quasinormal modes and null geodesics [61–63]. However, it should be noted that this correspondence has several limitations, as described in [62–64].

From this point onward in this section, we will compute quasinormal frequencies in units of the fixed radius of the event horizon, $r_0 = 1$, rather than fixing the mass of the black hole, M. The mass and radius of the event horizon are related by the following equation:

$$M = \frac{(r_0^2 + l_0^2)^{3/2}}{2r_0^2}. \tag{22}$$

This equation allows us to switch between the units $r_0 = 1$ and $M = 1$. The units of the fixed event horizon are more convenient for the application of the Frobenius method, which requires a precise understanding of the singular points of the differential equation under consideration.

The fundamental quasinormal modes for the test scalar field ($\ell = n = 0$), electromagnetic field ($\ell = 1$, $n = 0$), and Dirac field ($\ell = 1/2$, $n = 0$) are presented in Tables I–III for various values of l_0. These values are chosen in such a way that the range between the Schwarzschild limit $l_0 = 0$ and the last value before the near extreme one $l_0 = 0.707107$ is split into equal parts, in order to track smooth dependence of the frequencies on l_0. The accurate values are obtained using the convergent Frobenius method [28] for scalar and electromagnetic fields, while for the Dirac field, which has a nonpolynomial wave equation, we were limited to using the WKB method. A comparison of these values with earlier published results [4,7] reveals that the ordinary sixth order WKB data (without Padé approximants) is inaccurate, with a relative error reaching approximately 10%. However, the advanced WKB method with Padé approximants considered here [44] shows much better agreement with accurate quasinormal frequencies, reducing the relative error to a small fraction of 1%. The Frobenius method can only be applied to polynomial forms of the metric function and

TABLE I. Fundamental quasinormal modes for the scalar perturbations ($n = 0$, $\ell = 0$).

	WKB			Frobenius	
l_0	Sixth	Sixth (Pade 5)	Sixth (Pade 6)	20th order	24th order
0	$0.220934 - 0.201633i$	$0.221584 - 0.209367i$	$0.221357 - 0.208847i$	$0.220910 - 0.209791i$	$0.220910 - 0.209791i$
0.07698	$0.220288 - 0.199177i$	$0.220818 - 0.206828i$	$0.220585 - 0.206324i$	$0.220146 - 0.207248i$	$0.220146 - 0.207248i$
0.15396	$0.218078 - 0.192489i$	$0.218398 - 0.199312i$	$0.218146 - 0.198876i$	$0.217717 - 0.199765i$	$0.217717 - 0.199765i$
0.23094	$0.214096 - 0.182285i$	$0.213780 - 0.187430i$	$0.213541 - 0.187065i$	$0.213239 - 0.187801i$	$0.213239 - 0.187801i$
0.30792	$0.209605 - 0.165605i$	$0.205935 - 0.172526i$	$0.205928 - 0.172054i$	$0.206151 - 0.172156i$	$0.206151 - 0.172156i$
0.3849	$0.203168 - 0.140512i$	$0.195809 - 0.154749i$	$0.195900 - 0.154227i$	$0.195821 - 0.154042i$	$0.195821 - 0.154042i$
0.46188	$0.186592 - 0.119218i$	$0.183120 - 0.134872i$	$0.182642 - 0.134402i$	$0.181717 - 0.135270i$	$0.181717 - 0.135270i$
0.53886	$0.166413 - 0.106640i$	$0.164673 - 0.118464i$	$0.164432 - 0.118343i$	$0.164121 - 0.118732i$	$0.164119 - 0.118735i$
0.61584	$0.149688 - 0.096004i$	$0.147642 - 0.106578i$	$0.147526 - 0.106419i$	$0.146968 - 0.106725i$	$0.146995 - 0.106719i$
0.69282	$0.134525 - 0.086147i$	$0.132643 - 0.095711i$	$0.132524 - 0.095546i$	$0.132241 - 0.0959643i$	$0.132129 - 0.0958409i$
0.707107	$0.131840 - 0.084424i$	$0.129995 - 0.093798i$	$0.129879 - 0.093637i$	$0.129702 - 0.0941100i$	$0.129521 - 0.0939448i$

TABLE II. Fundamental quasinormal modes for the electromagnetic perturbations ($n = 0$, $\ell = 1$).

	WKB			Frobenius	
l_0	Sixth	Sixth (Pade 5)	Sixth (Pade 6)	20th order	24th order
0	$0.496383 - 0.185274i$	$0.496509 - 0.184993i$	$0.496509 - 0.184961i$	$0.496527 - 0.184975i$	$0.496527 - 0.184975i$
0.069282	$0.494945 - 0.183682i$	$0.495092 - 0.183337i$	$0.495086 - 0.183305i$	$0.495104 - 0.183318i$	$0.495104 - 0.183318i$
0.138564	$0.490564 - 0.178948i$	$0.490767 - 0.178429i$	$0.490754 - 0.178398i$	$0.490772 - 0.178411i$	$0.490772 - 0.178411i$
0.207846	$0.483055 - 0.171211i$	$0.483353 - 0.170467i$	$0.483338 - 0.170434i$	$0.483353 - 0.170452i$	$0.483353 - 0.170452i$
0.277128	$0.472162 - 0.160742i$	$0.472577 - 0.159796i$	$0.472563 - 0.159759i$	$0.472572 - 0.159784i$	$0.472572 - 0.159784i$
0.34641	$0.457592 - 0.147991i$	$0.458107 - 0.146925i$	$0.458095 - 0.146889i$	$0.458099 - 0.146918i$	$0.458099 - 0.146918i$
0.415692	$0.439053 - 0.133649i$	$0.439614 - 0.132573i$	$0.439603 - 0.132545i$	$0.439605 - 0.132570i$	$0.439605 - 0.132570i$
0.484974	$0.416343 - 0.118720i$	$0.416890 - 0.117721i$	$0.416882 - 0.117704i$	$0.416881 - 0.117720i$	$0.416881 - 0.117720i$
0.554256	$0.389608 - 0.104530i$	$0.390103 - 0.103633i$	$0.390099 - 0.103626i$	$0.390100 - 0.103635i$	$0.390096 - 0.103636i$
0.623538	$0.359764 - 0.092365i$	$0.360192 - 0.091561i$	$0.360190 - 0.091559i$	$0.360256 - 0.0915651i$	$0.360201 - 0.0915712i$
0.69282	$0.328400 - 0.082759i$	$0.328778 - 0.082042i$	$0.328774 - 0.082038i$	$0.329444 - 0.0819892i$	$0.328945 - 0.0820359i$
0.707107	$0.321891 - 0.081076i$	$0.322262 - 0.080374i$	$0.322258 - 0.080369i$	$0.323296 - 0.0802851i$	$0.322542 - 0.0803561i$

effective potentials. To meet this requirement, we expand the metric function in terms of small l_0 (see Appendix for the explicit form of the expansion) and apply the Frobenius method to this expanded metric. We observe that the quasinormal frequencies calculated using the metric function expanded up to the 20th and 24th orders in l_0 are in excellent agreement (see Tables I and II). An example of the convergence in terms of l_0 is shown in Fig. 2.

TABLE III. Fundamental quasinormal modes for the Dirac perturbations ($n = 0$, $\ell = 1/2$).

	WKB		
l_0	Sixth	Sixth (Pade 5)	Sixth (Pade 6)
0	$0.366162 - 0.194105i$	$0.365943 - 0.193956i$	$0.365813 - 0.193991i$
0.07698	$0.364600 - 0.191742i$	$0.364392 - 0.191630i$	$0.364267 - 0.191664i$
0.15396	$0.359889 - 0.184810i$	$0.359702 - 0.184821i$	$0.359589 - 0.184851i$
0.23094	$0.351950 - 0.173766i$	$0.351761 - 0.174019i$	$0.351660 - 0.174036i$
0.30792	$0.340642 - 0.159328i$	$0.340367 - 0.159983i$	$0.340279 - 0.159978i$
0.3849	$0.325739 - 0.142490i$	$0.325228 - 0.143677i$	$0.325166 - 0.143648i$
0.46188	$0.306947 - 0.124700i$	$0.306169 - 0.126350i$	$0.306135 - 0.126322i$
0.53886	$0.284334 - 0.107994i$	$0.283432 - 0.109828i$	$0.283418 - 0.109814i$
0.61584	$0.259273 - 0.094155i$	$0.258320 - 0.095939i$	$0.258314 - 0.095930i$
0.69282	$0.233822 - 0.083456i$	$0.232929 - 0.085144i$	$0.232909 - 0.085107i$
0.707107	$0.229173 - 0.081764i$	$0.228298 - 0.083422i$	$0.228278 - 0.083383i$

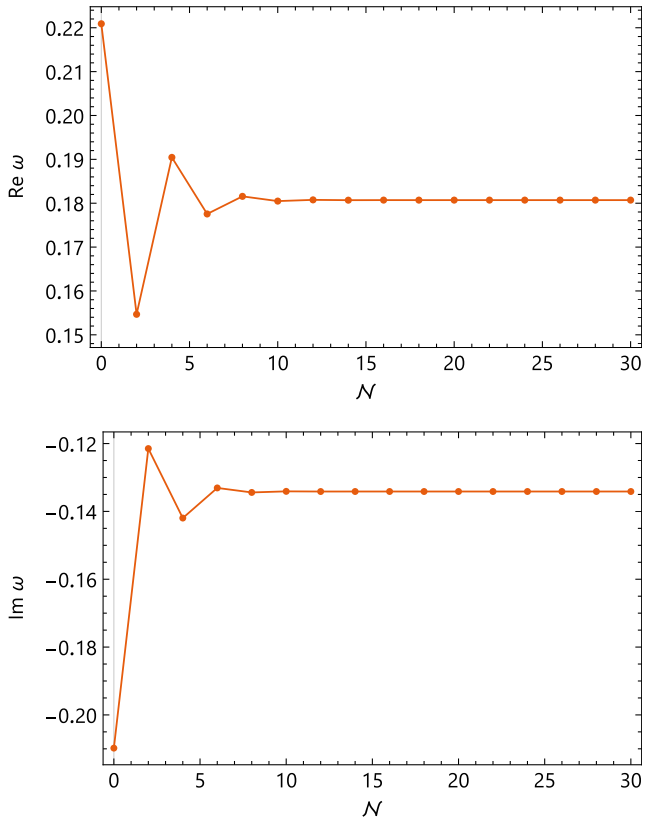

FIG. 2. An example of the convergence of the scalar field quasinormal modes ω calculated by the Frobenius method as the order of the expansion $\mathcal{N}$ in terms of small l_0 is increased ($n = 0$, $\ell = 0$) and $l_0 = 0.46669$.

The higher the overtone n one needs to find, the higher the order of expansion of the metric that should be used.

Integration of the wave equation in the time domain and subsequent extraction of dominant frequencies from the profile using the Prony method also confirm the accuracy of the Frobenius and WKB (with Padé) data. For instance, for the quasiextremal state $\ell_0 = 0.707107$ and $\ell = 0$ scalar perturbations, the frequency $\omega = 0.12958 - 0.09393i$ is extracted from the time-domain profile. This is in close agreement with the Frobenius method for the metric expanded up to the 24th order, which gives $\omega = 0.129521 - 0.0939448i$, and the sixth order WKB method with Padé approximants, which gives $\omega = 0.129879 - 0.093637i$. On the other hand, the usual sixth order WKB method produces an approximately 10% error in the damping rate.

At asymptotically late times, when the quasinormal ringing is suppressed by power-law tails, the Price decay law for the test scalar and gravitational fields [65] is fulfilled:

$$|\Psi| \sim t^{-(2\ell+3)}, \qquad t \to \infty. \tag{23}$$

This can be observed in Fig. 3.

The first several overtones exhibit the most interesting feature. They deviate from their Schwarzschild values at a significantly higher rate compared with the fundamental mode, and this rate increases with the overtone number (see Figs. 4 and 5). While the fundamental mode undergoes only a slight change, limited to moderate values of the quantum deformation parameter l_0 (as shown in Fig. 4), the real oscillation frequency of the sixth overtone decreases by more than twice its Schwarzschild limit.

This outburst of overtones occurs because the Bardeen spacetime differs from the Schwarzschild spacetime mainly in a region near the event horizon. This characteristic could potentially enable us to discern the quantum corrections near the horizon through the early phase of the quasinormal ringing, which includes contributions from the overtones [34,35]. It is important to note that if we consider the Bardeen spacetime as a deformation of the Schwarzschild black hole, this deformation is not highly localized and, therefore, is not related to the so-called

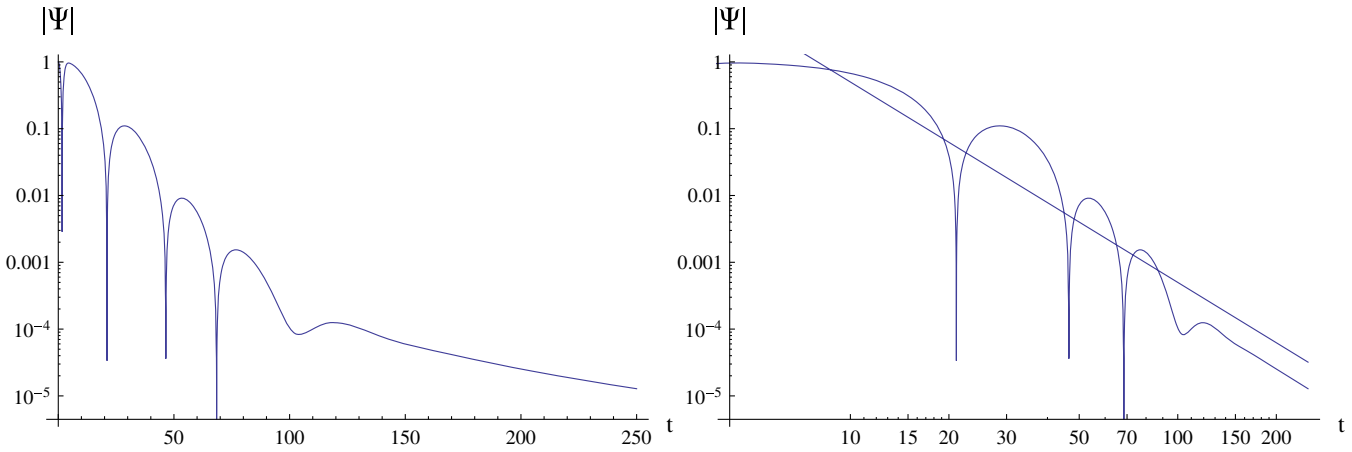

FIG. 3. Time-domain profile of the scalar field perturbations $\ell = 0$ for the quasiextremal Bardeen black hole $l_0 = 0.707107$; $r_0 = 1$. Left: semilogarithmic plot. Right: logarithmic plot with the line $\sim t^{-3}$.

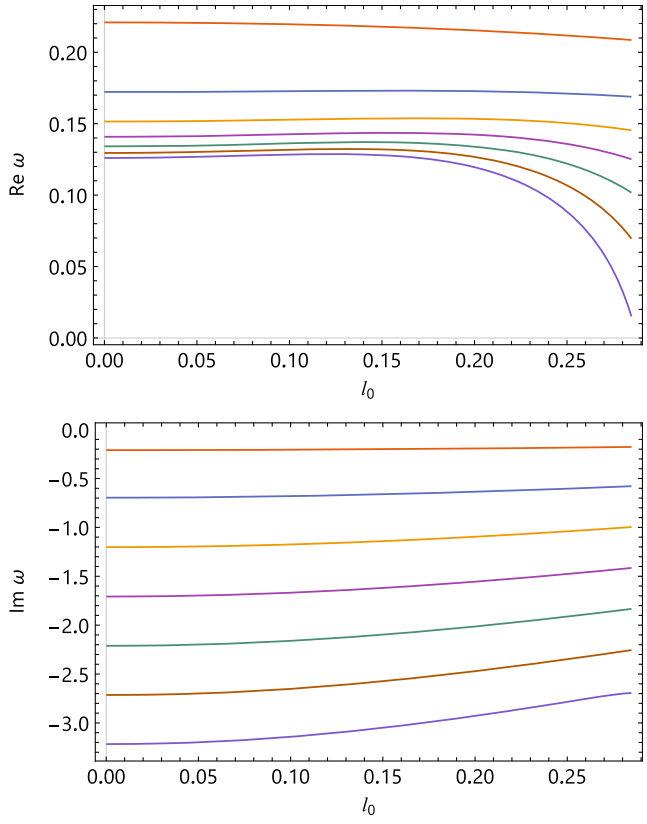

FIG. 4. Quasinormal frequencies for the scalar perturbations ($\ell = 0$) and n from 0 to 6.

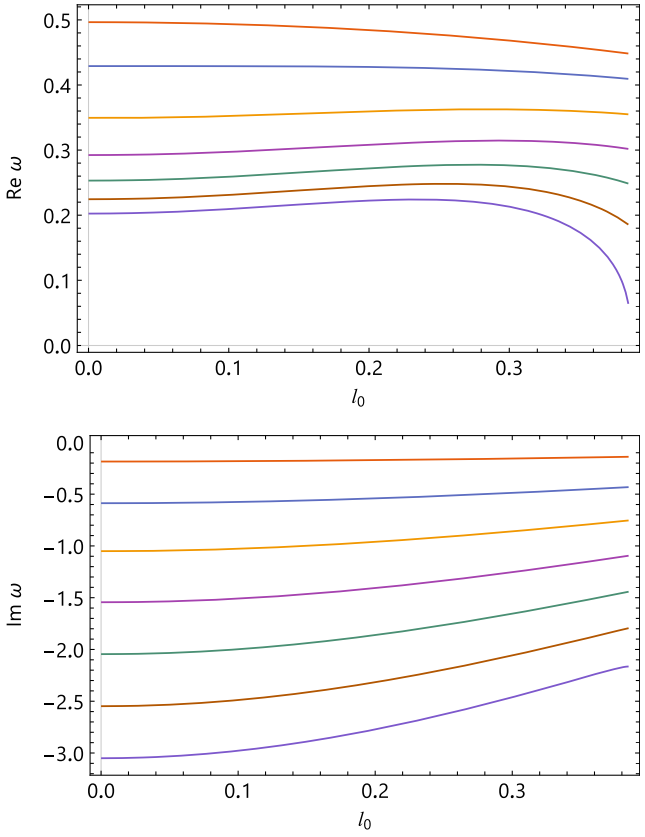

FIG. 5. Quasinormal frequencies for the electromagnetic perturbations ($\ell = 1$) and n from 0 to 6.

"high-frequency perturbations" (which actually refer to "highly localized deformation") discussed in [66] and subsequent works. The deformation of the Schwarzschild spacetime introduced by the parameter l_0 is smooth and extends over a neighborhood of the event horizon, gradually decaying as we move away from the black hole.

The significant decrease in the real oscillation frequencies of the overtones with increasing deformation parameter l_0 suggests the possibility of purely imaginary quasinormal modes in the spectrum at larger values of l_0. However, owing to the computational limitations, we were unable to find such modes as they would require much longer computation times. It is important to note that the quantum correction parameter is intended to represent a relatively small or at most moderate correction to the Schwarzschild spacetime. Therefore, the metric should remain sufficiently far from its extreme state, ensuring that the corrections remain within a reasonable range.

V. HAWKING RADIATION

It is essential to note that radiation from test fields surpasses that of gravitons: as is known using Schwarzschild black holes as an example, gravitons account for less than 2% of the total radiation flux, as illustrated in [67] and also summarized in Table I of [52].

Here we will assume that during sufficiently short periods of time the temperature of the black hole remains constant between the emission of two consecutive particles. According to this assumption, the system can be characterized by the canonical ensemble, which is extensively discussed in the literature (see, e.g., [68]). Consequently, the well-known Hawking formula for the energy emission rate [69] can be applied:

$$\frac{\mathrm{d}E}{\mathrm{d}t} = \sum_{\ell} N_{\ell} |\mathcal{A}_{\ell}|^2 \frac{\omega}{\exp\left(\omega/T_{\mathrm{H}}\right) \pm 1} \cdot \frac{\mathrm{d}\omega}{2\pi}, \tag{24}$$

where T_H is the Hawking temperature, $\mathcal{A}_\ell$ are gray-body factors, and N_ℓ are the multiplicity factors which depend on the number of species of particles and ℓ. The Hawking temperature is [69]

$$T = \left.\frac{f'(r)}{(4\pi)}\right|_{r=r_0}. \tag{25}$$

The dependence of the temperature on the parameter l_0 is shown in Fig. 6.

As long as we are considering the evaporation stage when the black hole is large enough, one can neglect emission of massive particles [70] as compared with

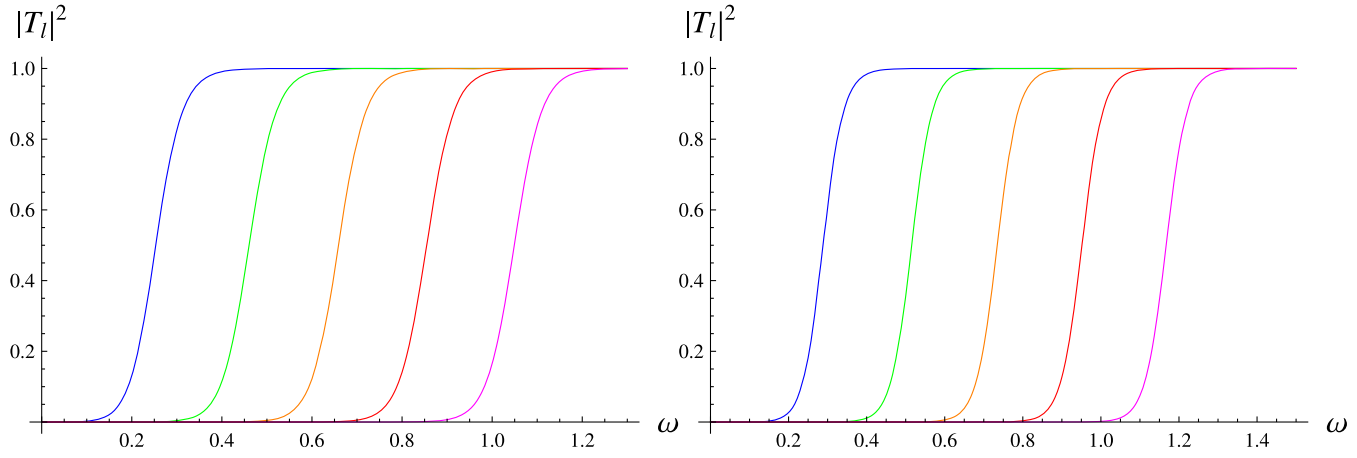

FIG. 6. Gray-body factors for the Maxwell field as a function of ω for the Schwarzschild solution (left panel) and the near extreme ($l_0 = 0.7$) Bardeen black hole (right panel) computed by the sixth order WKB approach for the first five multipoles $\ell = 1, 2, ..5$ from left to right.

massless ones. Accordingly, we will here consider only massless particles of the Standard Model, and, as was argued above, we neglect the emission of gravitons. Once the black hole is small enough, or, alternatively, the deformation parameter l_0/r_0 is large enough, massive particles, such as electrons and positrons, are emitted in an ultrarelativistic mode, that is, roughly at the same rate as massless neutrinos for each helicity.

The multiplicity factors for the 4D spherically symmetrical black holes consist of the number of degenerate m modes (which are $m = -\ell, -\ell + 1, ... - 1, 0, 1, ...\ell$, that is $2\ell + 1$ modes) multiplied by the number of species of particles, which in turn depends also on the number of polarizations and helicities of particles. Therefore, we have

$$N_\ell = 2(2\ell + 1) \qquad \text{(Maxwell)}, \tag{26}$$

$$N_\ell = 8\ell \qquad \text{(Dirac)}. \tag{27}$$

The multiplicity factor for the Dirac field is fixed taking into account both the "plus" and "minus" potentials related by Darboux transformations, which leads to an isospectral problem and the same gray-body factors for both chiralities. We will use here the "plus" potential, because the WKB results are more accurate for that case in the Schwarzschild limit.

The energy emitted makes the black hole mass decrease at the following rate [67]:

$$\frac{dM}{dt} = -\frac{\hbar c^4}{G^2}\frac{\alpha_0}{M^2} \approx -1.91 \times 10^{29}\alpha_0 \frac{\text{g}}{\text{s}} \cdot \left(\frac{\text{g}^2}{M_0^2}\right), \tag{28}$$

where we have restored the dimensional constants. Here $\alpha_0 = dE/dt$ is taken in units used in Table IV for a given initial mass M_0. Indeed, this can be seen by comparison of our data in the Schwarzschild limit with [67]. A relatively small difference with the Page's results (less than 2%) is due to the systematic error of the WKB method [46] and can be neglected, taking into account that the overall effect of deviation of the energy emission rate from the Schwarzschild limit achieves a few orders, i.e. the relative error is a few orders smaller than the effect.

From Table IV, it is evident that the energy emission rate dE/dt decreases by 3 orders of magnitude as the deformation parameter l_0 approaches the quasiextreme limit.

The effect observed in our current research can be attributed to two factors. The primary and dominant factor is the decrease in the Hawking temperature of the black hole when the quantum correction is introduced (see Fig. 9). The second factor is the gray-body coefficient. Analyzing the shape of the effective potentials of the Bardeen black hole shown in Fig. 1, it is evident that the height of the potential barrier increases with the inclusion of the quantum correction. Consequently, a taller effective potential reflects a larger portion of the initial radiation flow, contributing to the suppression of Hawking radiation. The examples of gray-body factors for the electromagentic and Dirac fields are shown in Figs. 6 and 7 respectively.

From Fig. 8, we observe that while the emission rate of the Maxwell field per unit frequency decreases significantly when the near-extreme quantum correction is applied, the peak of the radiation occurs at approximately the same frequency ω. Similar behavior is observed for the Dirac particles.

We have calculated the contributions of the first five multipoles ℓ. However, it is noteworthy that the contributions of only the first two multipoles are significant for the total energy emission rate. Therefore, higher multipoles can be safely neglected.

Such a strong attenuation of flux of the Hawking radiation could also be explained in an analytic way. The influence of the gray-body factors could be roughly estimated via the WKB arguments. Using Eq. (18) and the

TABLE IV. Energy emission rate dE/dt for the Bardeen black hole.

l_0/M	Maxwell	Dirac
0 ($\ell=1$)	0.0000335107	0.00015963
0 ($\ell=2$)	6.67916×10^{-7}	5.8691×10^{-6}
0 ($\ell=3$)	1.00693×10^{-8}	1.16695×10^{-7}
0 (total)	0.0000341888	0.000165617
0.1 ($\ell=1$)	0.0000323629	0.000155663
0.1 ($\ell=2$)	6.28544×10^{-7}	5.58669×10^{-6}
0.1 ($\ell=3$)	9.23148×10^{-9}	1.08274×10^{-7}
0.1 (total)	0.0000330008	0.00016136
0.2 ($\ell=1$)	0.0000290019	0.000144034
0.2 ($\ell=2$)	5.1916×10^{-7}	4.78308×10^{-6}
0.2 ($\ell=3$)	7.02324×10^{-9}	8.55366×10^{-8}
0.2 (total)	0.0000295282	0.000148904
0.3 ($\ell=1$)	0.0000236953	0.00012464
0.3 ($\ell=2$)	3.64925×10^{-7}	3.5915×10^{-6}
0.3 ($\ell=3$)	4.24242×10^{-9}	5.53788×10^{-8}
0.3 (total)	0.0000240645	0.000128288
0.4 ($\ell=1$)	0.0000169636	0.000102356
0.4 ($\ell=2$)	2.03653×10^{-7}	2.23439×10^{-6}
0.4 ($\ell=3$)	1.84218×10^{-9}	2.70179×10^{-8}
0.4 (total)	0.0000171691	0.000104618
0.5 ($\ell=1$)	9.71567×10^{-6}	0.0000658481
0.5 ($\ell=2$)	7.69549×10^{-8}	1.01073×10^{-6}
0.5 ($\ell=3$)	4.57759×10^{-10}	8.10308×10^{-9}
0.5 (total)	9.79308×10^{-6}	0.000066867
0.6 ($\ell=1$)	3.45285×10^{-6}	0.000031204
0.6 ($\ell=2$)	1.26319×10^{-8}	2.34735×10^{-7}
0.6 ($\ell=3$)	3.44314×10^{-11}	8.70239×10^{-10}
0.6 (total)	3.46552×10^{-6}	0.00003144
0.7 ($\ell=1$)	2.34399×10^{-7}	4.29524×10^{-6}
0.7 ($\ell=2$)	1.18349×10^{-10}	4.79822×10^{-9}
0.7 ($\ell=3$)	4.36355×10^{-14}	2.55798×10^{-12}
0.7 (total)	2.34517×10^{-7}	4.30004×10^{-6}

double expansion in terms of $1/L$ and l_0 we find in the leading orders of $1/L$ that

$$K \approx \frac{i(18M^2-l_0^2)(81M^4\omega^2-3M^2L^2-l_0^2L^2)}{108M^4L}. \tag{29}$$

Using the above equation in (19), one can see that the gray-body factors are suppressed exponentially as l_0 is turned on, so that we have

$$\mathcal{A}_\ell = \frac{1}{1+e^{\alpha(l_0,\omega,M,\ell)}}, \tag{30}$$

where

$$\alpha(l_0,\omega,M,\ell) = \frac{-108\pi M^2\omega^2+4\pi\ell^2+4\pi\ell+\pi}{2(2\ell+1)} + \frac{l_0^2(108\pi M^2\omega^2+20\pi\ell^2+20\pi\ell+5\pi)}{36M^2(2\ell+1)} + O(l_0^4). \tag{31}$$

The above formula could be extended to higher orders beyond the eikonal approximation according to [71] showing great concordance with the sixth order WKB numerical data already at the first orders of expansion in terms of $1/L$.

However, the essential factor of strong decreasing of the total flow at all frequencies ω remains the temperature which also exponentially suppresses the emission as can be seen from Eq. (24) and Fig. 9. One can see that as l_0 approaches its extreme value $l_o^{\rm ext}\approx 0.7698M$, the Hawking temperature vanishes, so the energy emission rate goes to zero. This is the main factor of suppression in the regime of relatively large l_0.

As there are currently several concurrent models for quantum corrections to black hole spacetime, an important question arises: to what extent does the suppression of Hawking radiation depend on the specific model of quantum correction? Based on our current knowledge, in the majority of cases, corrections to Einstein gravity in four or higher dimensions lead to the effect of suppression. For instance, in Einsteinian cubic gravity, the Maxwell field experiences suppression of up to 2 orders [72], while the Dirac field is suppressed by approximately 1 order. In the $4D$-Einstein-Gauss-Bonnet theory, suppression occurs by a few times even at small values of the coupling constant [56]. The Einstein-Weyl gravity shows a slight enhancement at a small coupling, owing to larger gray-body factors, but experiences considerable suppression at larger coupling, where the temperature plays the main role [52]. Finally, it is worth noting that in the higher-dimensional Einstein-Gauss-Bonnet theory, there is a few orders' suppression when compared with the D-dimensional Einstein theory [55].

In the case of apparent enhancement in the Einstein-dilaton-Gauss-Bonnet theory [64], a comparison with the Schwarzschild case must be made not in units of the radius of the event horizon, but appropriately rescaled to the units of mass. An evidently opposite effect has been observed in the nonperturbative Kazakov-Solodukhin model of quantum correction [57,73]. However, in this model, the Hawking temperature of the quantum-corrected black hole remains the same as in the Schwarzschild case, which raises some skepticism regarding the possibility that the calculated correction is dominant. The above observations indicate that quantum corrections may indeed lead to the suppression of Hawking radiation. However, it is important to acknowledge that a final, single, and noncontradictory model for quantum black holes has not yet been established.

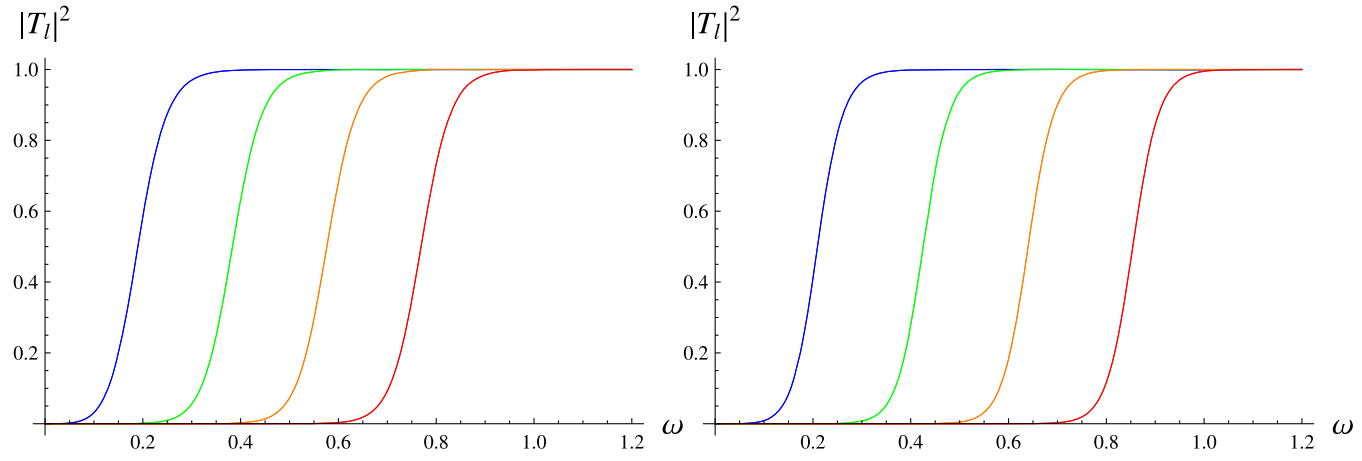

FIG. 7. Gray-body factors for the Dirac field as a function of ω for the Schwarzschild solution (left panel) and the near extreme ($l_0 = 0.7$) Bardeen black hole (right panel) computed by the third order WKB approach for the first five multipoles $\ell = 1, 2, ..5$ from left to right.

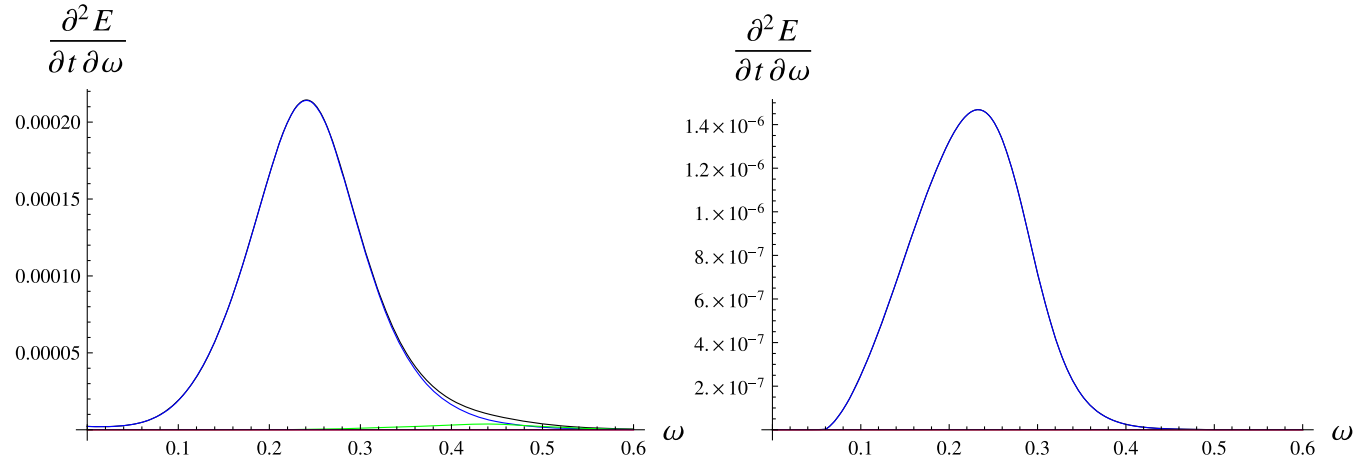

FIG. 8. Energy emission rates per unit of frequency for the Maxwell field for the Schwarzschild spacetime (left plot) and for the near extreme Bardeen black hole $l_0 = 0.7$ (right plot). One can see that the contribution consists almost completely from the first multipole $\ell = 1$ (blue, top) and $\ell = 2$ (yellow, bottom), while higher multipoles could be neglected. The black line is for the total emission rate summed over the first five multipoles.

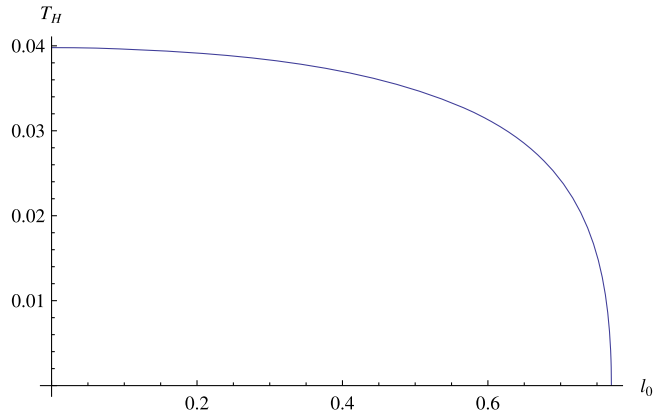

FIG. 9. Temperature of the Bardeen black hole at fixed mass $M = 1$ as a function of the deformation parameter l_0.

Further research and theoretical developments are still needed in this area.

VI. CONCLUSIONS

The Bardeen spacetime characterizes a regular black hole featuring a de Sitter core in place of a central singularity. By interpreting this spacetime as the metric of a quantum-corrected black hole within the framework of string T duality [29], we conducted a comprehensive analysis of the quasinormal spectrum for scalar, electromagnetic, and Dirac fields in this background. Our investigation revealed that some previous studies focusing on the fundamental mode exhibited inaccuracies, allowing for a relative error of up to 10%. However, our primary findings pertain to the calculations of overtones, which probe the

geometry near the event horizon and thus play a crucial role in discerning potential quantum corrections through observations of classical radiation emitted by black holes. Notably, we observed that the initial few overtones deviate from their Schwarzschild values at a significantly higher rate compared with the fundamental mode. This deviation stems from the quantum correction-induced deformation of the Schwarzschild spacetime.

Additionally, we derived an analytical expression for the quasinormal modes in the eikonal regime and established the decay law at asymptotically late times.

Furthermore, we computed the gray-body factors and energy emission rates for massless fields surrounding the Bardeen black hole. Our analysis revealed that the quantum correction leads to a significant suppression of the Hawking radiation intensity by several orders of magnitude. This suppression arises from two factors: a decrease in the Hawking temperature and a smaller gray-body factor.

Our study on the Hawking evaporation of the Bardeen black hole holds potential significance in estimating the number of primordial black holes formed during the early Universe. Specifically, for $M \lesssim 10^{15} g$, the evaporation of primordial black holes is predominantly constrained by big bang nucleosynthesis [74]. Therefore, the quantum correction examined in this study could serve as one of the mechanisms, alongside those considered in [75], that changes the speed of the black hole evaporation, potentially influencing the constraints imposed by big bang nucleosynthesis on the abundance of primordial black holes.

There are several avenues for extending our work. Firstly, one could investigate the Hawking radiation of massive particles to obtain a more accurate understanding of the radiation process during the later stages of black hole evaporation. Secondly, the decreasing real oscillation frequencies of the overtones at moderate values of l_0 suggest that, at a sufficiently large deformation parameter, some of these overtones may become purely imaginary, corresponding to nonoscillatory modes. However, owing to the slow convergence of the procedure in this regime, we were unable to explore this phenomenon within a reasonable computation time. It is possible that alternative methods, such as the Bernstein polynomial method [76,77], which are more effective at finding purely imaginary modes, could offer a solution to this challenge. Finally, quasinormal frequencies of massless fields could be complemented by the analysis of massive fields, which may have arbitrary long-lived modes called quasiresonances [78,79]. It would be interesting to understand how these long-lived modes affect the overtones' structure.

ACKNOWLEDGMENTS

The authors would like to acknowledge useful discussions with Alexander Zhidenko. They would also like to acknowledge the support of the Research Centre for Theoretical Physics and Astrophysics, Institute of Physics, Silesian University in Opava. D. O. thanks the financial support of the internal grant of the Silesian University in Opava SGS/30/2023. B. A. acknowledges support by Grants No. F-FA-2021-432 and No. MRB-2021-527 from the Agency for Innovative Development of Uzbekistan and Erasmus + project toward his stay at the Silesian University in Opava.

APPENDIX

The expansion of the metric function $f(r)$ in terms of small l_0 has the following form:

$$f(r) = \left(1 - \frac{2M}{r}\right) + \frac{3l_0^2 M}{r^3} - \frac{15 l_0^4 M}{4r^5} + \frac{35 l_0^6 M}{8r^7} - \frac{315 l_0^8 M}{64 r^9} + \frac{693 l_0^{10} M}{128 r^{11}} - \frac{3003 l_0^{12} M}{512 r^{13}} + \frac{6435 l_0^{14} M}{1024 r^{15}} - \frac{109395 l_0^{16} M}{16384 r^{17}} + \frac{230945 l_0^{18} M}{32768 r^{19}} - \frac{969969 l_0^{20} M}{131072 r^{21}} + \frac{2028117 l_0^{22} M}{262144 r^{23}} - \frac{16900975 l_0^{24} M}{2097152 r^{25}} + O(l_0^{26}). \quad \text{(A1)}$$

[1] J. M. Bardeen, in *Abstracts of the 5th International Conference on Gravitation and the Theory of Relativity (GR5), Tbilisi, USSR, 1968*, edited by V. A. Fock *et al.* (Tbilisi University Press, 1968), p. 174.
[2] E. Ayon-Beato and A. Garcia, Phys. Lett. B **493**, 149 (2000).
[3] K. A. Bronnikov, Phys. Rev. D **63**, 044005 (2001).
[4] S. Fernando and J. Correa, Phys. Rev. D **86**, 064039 (2012).
[5] N. Breton and L. A. Lopez, Phys. Rev. D **94**, 104008 (2016).
[6] A. Flachi and J. P. S. Lemos, Phys. Rev. D **87**, 024034 (2013).
[7] B. Toshmatov, A. Abdujabbarov, Z. Stuchlík, and B. Ahmedov, Phys. Rev. D **91**, 083008 (2015).
[8] B. Toshmatov, Z. Stuchlík, B. Ahmedov, and D. Malafarina, Phys. Rev. D **99**, 064043 (2019).
[9] D. Mahdavian Yekta, M. Karimabadi, and S. A. Alavi, Ann. Phys. (Amsterdam) **434**, 168603 (2021).
[10] H. Liu, C. Zhang, Y. Gong, B. Wang, and A. Wang, Phys. Rev. D **102**, 124011 (2020).

[11] M. Mondal, A. K. Yadav, P. Pradhan, S. Islam, and F. Rahaman, Int. J. Mod. Phys. D **30**, 2150095 (2021).
[12] A. Rincón and V. Santos, Eur. Phys. J. C **80**, 910 (2020).
[13] L. A. López and V. Ramírez, Eur. Phys. J. Plus **138**, 120 (2023).
[14] S. C. Ulhoa, Braz. J. Phys. **44**, 380 (2014).
[15] C. F. B. Macedo, L. C. B. Crispino, and E. S. de Oliveira, Int. J. Mod. Phys. D **25**, 1641008 (2016).
[16] W. Wahlang, P. A. Jeena, and S. Chakrabarti, Int. J. Mod. Phys. D **26**, 1750160 (2017).
[17] M. Saleh, B. B. Thomas, and T. C. Kofane, Eur. Phys. J. C **78**, 325 (2018).
[18] S. Dey and S. Chakrabarti, Eur. Phys. J. C **79**, 504 (2019).
[19] K. Jusufi, M. Amir, M. S. Ali, and S. D. Maharaj, Phys. Rev. D **102**, 064020 (2020).
[20] J. Rayimbaev, B. Majeed, M. Jamil, K. Jusufi, and A. Wang, Phys. Dark Universe **35**, 100930 (2022).
[21] S. R. Wu, B. Q. Wang, and Z. W. Long, arXiv:2207.05907.
[22] Q. Sun, Q. Li, Y. Zhang, and Q.-Q. Li, arXiv:2302.10758.
[23] B. K. Vishvakarma, D. V. Singh, and S. Siwach, Eur. Phys. J. Plus **138**, 536 (2023).
[24] Y. Liu and X. Zhang, arXiv:2305.02642.
[25] B. P. Abbott *et al.* (LIGO Scientific and Virgo Collaborations), Phys. Rev. Lett. **116**, 061102 (2016).
[26] D. T. Son and A. O. Starinets, Annu. Rev. Nucl. Part. Sci. **57**, 95 (2007).
[27] R. A. Konoplya and A. Zhidenko, Rev. Mod. Phys. **83**, 793 (2011).
[28] E. W. Leaver, Proc. R. Soc. A **402**, 285 (1985).
[29] P. Nicolini, E. Spallucci, and M. F. Wondrak, Phys. Lett. B **797**, 134888 (2019).
[30] T. Padmanabhan, Phys. Rev. D **57**, 6206 (1998).
[31] R. V. Maluf and J. C. S. Neves, Int. J. Mod. Phys. D **28**, 1950048 (2018).
[32] V. Cardoso, E. Franzin, and P. Pani, Phys. Rev. Lett. **116**, 171101 (2016); **117**, 089902(E) (2016).
[33] T. Damour and S. N. Solodukhin, Phys. Rev. D **76**, 024016 (2007).
[34] R. A. Konoplya and A. Zhidenko, arXiv:2209.00679.
[35] M. Giesler, M. Isi, M. A. Scheel, and S. Teukolsky, Phys. Rev. X **9**, 041060 (2019).
[36] R. A. Konoplya, J. Cosmol. Astropart. Phys. 07 (2023) 001.
[37] R. A. Konoplya, Z. Stuchlik, A. Zhidenko, and A. F. Zinhailo, Phys. Rev. D **107**, 104050 (2023).
[38] R. A. Konoplya, Phys. Rev. D **107**, 064039 (2023).
[39] R. A. Konoplya, A. F. Zinhailo, J. Kunz, Z. Stuchlik, and A. Zhidenko, J. Cosmol. Astropart. Phys. 10 (2022) 091.
[40] A. Borde, Phys. Rev. D **50**, 3692 (1994).
[41] B. F. Schutz and C. M. Will, Astrophys. J. Lett. **291**, L33 (1985).
[42] S. Iyer and C. M. Will, Phys. Rev. D **35**, 3621 (1987).
[43] R. A. Konoplya, Phys. Rev. D **68**, 024018 (2003).
[44] J. Matyjasek and M. Opala, Phys. Rev. D **96**, 024011 (2017).
[45] Y. Hatsuda, Phys. Rev. D **101**, 024008 (2020).
[46] R. A. Konoplya, A. Zhidenko, and A. F. Zinhailo, Classical Quantum Gravity **36**, 155002 (2019).
[47] H.-P. Nollert, Phys. Rev. D **47**, 5253 (1993).
[48] A. Zhidenko, Phys. Rev. D **74**, 064017 (2006).
[49] A. Rostworowski, Acta Phys. Pol. B **38**, 81 (2007), https://www.actaphys.uj.edu.pl/R/38/1/81/pdf.
[50] C. Gundlach, R. H. Price, and J. Pullin, Phys. Rev. D **49**, 883 (1994).
[51] Wolfram Research, Inc., Mathematica, Version 13.3, Champaign, IL, 2023, https://www.wolfram.com/mathematica.
[52] R. A. Konoplya and A. F. Zinhailo, Phys. Rev. D **99**, 104060 (2019).
[53] One of the two effective potentials for the Dirac perturbations has a negative gap, but it is isospectral to the other, which is positive definite.
[54] R. A. Konoplya, arXiv:2308.02850.
[55] R. A. Konoplya and A. Zhidenko, Phys. Rev. D **82**, 084003 (2010).
[56] R. A. Konoplya and A. F. Zinhailo, Phys. Lett. B **810**, 135793 (2020).
[57] K. A. Bronnikov and R. A. Konoplya, arXiv:2306.11083.
[58] V. Ferrari and B. Mashhoon, Phys. Rev. D **30**, 295 (1984).
[59] A. Zhidenko, Classical Quantum Gravity **21**, 273 (2004).
[60] M. S. Churilova, R. A. Konoplya, and A. Zhidenko, Phys. Rev. D **105**, 084003 (2022).
[61] V. Cardoso, A. S. Miranda, E. Berti, H. Witek, and V. T. Zanchin, Phys. Rev. D **79**, 064016 (2009).
[62] R. A. Konoplya and Z. Stuchlík, Phys. Lett. B **771**, 597 (2017).
[63] R. A. Konoplya, Phys. Lett. B **838**, 137674 (2023).
[64] R. A. Konoplya, A. F. Zinhailo, and Z. Stuchlík, Phys. Rev. D **99**, 124042 (2019).
[65] R. H. Price, Phys. Rev. D **5**, 2439 (1972).
[66] H.-P. Nollert, Phys. Rev. D **53**, 4397 (1996).
[67] D. N. Page, Phys. Rev. D **13**, 198 (1976).
[68] P. Kanti, Int. J. Mod. Phys. A **19**, 4899 (2004).
[69] S. W. Hawking, Commun. Math. Phys. **43**, 199 (1975); **46**, 206(E) (1976).
[70] A. B. Gaina, Sov. Phys. J. **28**, 682 (1985).
[71] R. A. Konoplya and A. Zhidenko, arXiv:2309.02560.
[72] R. A. Konoplya, A. F. Zinhailo, and Z. Stuchlik, Phys. Rev. D **102**, 044023 (2020).
[73] D. I. Kazakov and S. N. Solodukhin, Nucl. Phys. **B429**, 153 (1994).
[74] B. Carr, K. Kohri, Y. Sendouda, and J. Yokoyama, Rep. Prog. Phys. **84**, 116902 (2021).
[75] G. Franciolini and P. Pani, arXiv:2304.13576.
[76] S. Fortuna and I. Vega, arXiv:2003.06232.
[77] R. A. Konoplya and A. Zhidenko, Phys. Rev. D **107**, 044009 (2023).
[78] A. Ohashi and M.-a. Sakagami, Classical Quantum Gravity **21**, 3973 (2004).
[79] R. A. Konoplya and A. V. Zhidenko, Phys. Lett. B **609**, 377 (2005).